

Wave damping by flexible marsh plants influenced by current

Xiaoxia Zhang  ^{1,2,3,*} and Heidi Nepf ^{3,†}

¹*State Key Laboratory of Coastal and Offshore Engineering, Dalian University of Technology, Dalian, Liaoning 116024, China*

²*State Key Laboratory of Hydraulics and Mountain River Engineering, Sichuan University, Chengdu, Sichuan 610065, China*

³*Department of Civil and Environmental Engineering, Massachusetts Institute of Technology, Cambridge, Massachusetts 02139, USA*



(Received 4 August 2021; accepted 31 August 2021; published 13 October 2021)

This study considered how the presence of current impacted wave dissipation within a meadow of flexible marsh plants. A wave-damping model was developed from a prediction of current- and wave-induced force on individual plants. The model was validated with laboratory experiments. Wave decay was measured over a meadow of flexible model plants geometrically similar to *Spartina alterniflora* with and without a following current. Consistent with previous observations, the wave energy dissipation depended on the ratio of current velocity (U_c) to wave velocity (U_w). Compared to the same pure wave condition, wave energy dissipation was enhanced by large U_c/U_w but can be decreased for small U_c/U_w . Once validated, the wave-damping model was used to explore a wider range of wave, current, and meadow conditions in order to illustrate the influence of reconfiguration on wave forces; the impact of current on wave group velocity; and the modification of in-canopy time-mean and wave orbital velocity associated with canopy drag.

DOI: [10.1103/PhysRevFluids.6.100502](https://doi.org/10.1103/PhysRevFluids.6.100502)

I. INTRODUCTION

Salt marshes are efficient in dissipating wave energy [1–3], reducing current [4,5], and decreasing flood magnitude [6]. For example, coastal marshes reduced flood damage associated with Hurricane Sandy by 625 million USD [7]. The dissipation of hydrodynamic energy can reduce erosion [8] and promote sedimentation inside marshes [9], which is a feedback needed to maintain marshes through sea-level rise. The combined effects of vegetation-flow-sediment interaction make salt marsh a natural defense against stronger and more frequent coastal storm events brought by climate change [10–13]. Coastal managers are advocating for the restoration and management of marshes as natural infrastructure [10–13]. However, accurate methods for estimating the value of marsh coastal defense are needed to facilitate shifts in policy and management [14]. The goal of this work was to improve the prediction of wave dissipation by coastal marsh, which is an important element of the coastal defense function.

Many previous studies have quantified wave dissipation without current by representing vegetation as rigid cylinders and fitting empirical drag coefficients [15–17]. However, these fitted drag coefficients cannot be confidently applied to other sites because their dependence on real plant morphology, mechanical properties, meadow density, and wave conditions is not clearly understood. Marsh plants are flexible and thus can bend in response to current and move continuously with

*xxzhang@dlut.edu.cn

†hmnepf@mit.edu

waves, both of which are called reconfiguration, which reduces the frontal area and decreases the relative velocity between the plant and the fluid, both of which reduce the force on the flexible plant compared to a rigid plant of the same morphology [18,19]. The reduction in drag on individual plants decreases the wave dissipation by a meadow of plants [20,21]. The wave-induced force on a flexible plant element, F_d , can be described by two dimensionless parameters [19],

$$\frac{F_d}{F_r} \sim (\text{Ca}L)^{-1/4}, \quad (1)$$

in which F_r is the force on a rigid plant with the same morphology. The Cauchy number Ca is the ratio of hydrodynamic force to restoring force due to plant rigidity. L is the ratio of plant length, l , to wave orbital excursion, A_w ($=U_w/\omega$, with U_w the wave orbital velocity and ω the wave angular frequency).

$$\text{Ca} = \frac{\rho A U_{\max}^2}{EI/l^2}, \quad (2)$$

$$L = \frac{l}{A_w}. \quad (3)$$

Here, ρ is the water density, A is the frontal area, E is the elastic modulus, I is the second moment of area, and U_{\max} is the maximum horizontal velocity. Note that Ref. [19] defined the Cauchy number using the wave velocity, U_w , but in this study Eq. (2) was adapted for conditions with combined waves and current using $U_{\max} = U_w + U_c$, with current U_c . The scaling equation (1) is theoretically valid for $\text{Ca}L > 1$ and $L \gg 1$ [19,22,23] and experimentally shown to work for $\text{Ca} > 1$ and $L > 0.5$ [21,24]. Based on this, Eq. (1) was used for $L > 1$ and $\text{Ca}L > 1$ in this study, but for $\text{Ca}L < 1$ the plant drag reduction is negligible, i.e., $F_d = F_r$. For marsh plants, buoyancy does not significantly impact plant posture [25] and will not be considered in this study.

Unlike most previous studies, we consider the real morphology of marsh plants, which are composed of flexible leaves and a comparatively more rigid stem, both of which have been noted to contribute to wave damping [26,27]. The geometry and flexibility of marsh plants vary between species and can depend on the hydrodynamic environment [28]. The leaves often contribute most of the wave drag due to their greater frontal area compared to the stem [25]. The impact of reconfiguration on both the leaf and stem drag can be captured by the scale law shown in Eq. (1), through which the impact of reconfiguration on the full plant drag has been predicted [25].

In many situations, waves are accompanied by current, but a handful of studies have considered wave damping by plants under the influence of current (Table 1). Studies using rigid cylinders [29–31] suggest that when current is present, wave dissipation can be increased or decreased compared to pure waves, depending on the current direction and ratio of current to wave velocity, U_c/U_w . Specifically, with following currents (propagating in the same direction as the wave), wave dissipation increased when U_c/U_w was larger than a transition value, but decreased when U_c/U_w was smaller than the transition value [29,31]. Opposing currents were reported to increase the wave damping [31]. An increase in wave damping under opposing currents was also observed in experiments with live marsh plants [32–34]. However, a following current decreased wave damping by flexible mimics of seagrass for $U_c/U_w < 0.5$ [35] and by live marsh plants for $U_c/U_w = 0.5$ to 1.5 [32–34]. Based on field measurements, Ref. [36] showed that wave damping at comparable water depths during ebb tide (opposing current) was smaller than under flood tide (following current), which contradicted the previous observations that an opposing current enhanced wave dissipation [31,33]. While these studies bring attention to the effect of current on wave damping, they did not consider in detail the role of plant flexibility or leaf structure. The goal of this study was to consider all three factors: flexibility, leaves, and current, and to develop a predictive model that reflects all three, which has not, to the authors knowledge, been done before.

TABLE I. Previous studies of wave dissipation by vegetation under the influence of current. Subscripts l and s denote leaf and stem, respectively. D is stem diameter, b is leaf width, and E is elastic modulus. N_s and N_l are plants/m² and number of leaves per plant, respectively.

| Publication | Vegetation properties | U_c/U_w | Current | Wave | Main results |
|---------------------------|--|-----------|------------------------|---------------|---|
| Li and Yan [30] | Flume, semirigid rubber rods $N_s = 1111$, $l_s = 15$ cm, $D = 6$, 8 mm | 1.5–3.5 | Following | Regular | Following current increased wave dissipation |
| Paul <i>et al.</i> [35] | Flume, flexible and stiff mimics $N_s = 500$ to 8000, $l_l = 10, 15, 30$ cm, $b = 1.8, 2.2$ mm | <0.5 | Following | Regular | Following current reduced wave dissipation |
| Hu <i>et al.</i> [29] | Flume, rigid cylinders $N_s = 62, 139$, and 556, $l_s = 36$ cm, $D = 1$ cm | 0–5.4 | Following | Regular | Following current increased wave dissipation for $U_c/U_w > 0.65$ to 1.25, otherwise decreased |
| Lara <i>et al.</i> [32] | Flume, live | 0.5–1.4 | Following | Regular | Opposing current increased and |
| Losada <i>et al.</i> [33] | <i>Puccinellia maritima</i> | | and | and irregular | following current decreased |
| Maza <i>et al.</i> [34] | | | opposing | | wave dissipation |
| | $N_s = 2436, 1389$, and 877, $l_s = 47$ cm, $E_s = 13$ MPa, $l_l = 23$ cm, $b = 0.3$ cm, $N_l = 5.5$, $E_l = 7.8$ MPa | | | | |
| | Flume, live <i>Spartina anglica</i> $N_s = 729$ and 430, $l_s = 28$ cm, $E_s = 164$ MPa, $l_l = 18$ cm, $b = 0.6$ cm, $N_l = 5$, $E_l = 78$ MPa | | | | |
| Garzon <i>et al.</i> [36] | Field, <i>Spartina</i> $N_s = 344$, $l_s = 71$ cm, $D = 5$ mm | 0.4–3.3 | Alongshore and tidal | Irregular | Following current, associated with higher incoming wave height, exhibited greater wave dissipation than opposing current |
| Yin <i>et al.</i> [31] | Flume, rigid cylinders $N_s = 399$, $l_s = 70$ cm, $D = 2$ cm | 0–2.7 | Following and opposing | Regular | Following current decreased wave dissipation for $U_c/U_w < 0.37$ to 1.54, otherwise increased; opposing current increased wave dissipation to greater extent |

TABLE I. (*Continued.*)

| Publication | Vegetation properties | U_c/U_w | Current | Wave | Main results |
|-------------------------|---|-----------|------------------------|----------|---|
| Zhao <i>et al.</i> [37] | Flume, rigid cylinders $N_s = 278$, $l_s = 60$ cm, $D = 5$ mm | 0.2–1.2 | Following and opposing | Solitary | Following current increased wave dissipation; opposing current increased (decreased) wave dissipation for large (small) U_c/U_w |

II. PREDICTION OF WAVE DISSIPATION IN PRESENCE OF CURRENT

A. Force on a marsh plant

Marsh plants consist of N_l flexible leaves distributed around and along a flexible stem. For pure wave conditions, wave-induced force on a marsh plant, F_d , can be represented by the sum of forces on leaves and stem, each of which obey Eq. (1) [25].

$$F_d(t) = \underbrace{F_{r,l}(t)\{C_s N_l K_l (\text{Ca}_l L_l)^{-1/4}\}}_{F_l(t) \text{ leaf force}} + \underbrace{F_{r,s}(t)\{K_s (\text{Ca}_s L_s)^{-1/4}\}}_{F_s(t) \text{ stem force}}, \quad (4)$$

in which $F_{r,l}$ and $F_{r,s}$ are the time-varying forces on a rigid leaf and stem, respectively. Subscript l and s denote variables for leaf and stem, respectively. The Cauchy number and length ratio are defined for a flat leaf (Ca_l , L_l) and cylindrical stem (Ca_s , L_s) as in Eqs. (2) and (3), using their respective dimensions. The sheltering coefficient C_s quantifies the reduction in leaf force due to sheltering from other leaves and the stem. $C_s = 0.6$ was determined experimentally [25]. $K_l = 1$ [21] and $K_s = 1.2$ [38] are constants related to structure geometry. The force on a rigid vertical circular stem $F_{r,s}$ and a rigid vertical flat leaf $F_{r,l}$ are, respectively,

$$F_{r,s}(t) = \frac{1}{2} \rho C_{D,s} D l_s |U(t)| U(t) + \rho C_{M,s} \frac{\pi D^2}{4} l_s \frac{\partial U(t)}{\partial t}, \quad (5a)$$

$$F_{r,l}(t) = \frac{1}{2} \rho C_{D,l} b l_l |U(t)| U(t) + \rho C_{M,l} b d l_l \frac{\partial U(t)}{\partial t}, \quad (5b)$$

in which C_D and C_M are the drag and inertial coefficients, respectively. D is stem diameter, b is leaf width, and d is leaf thickness. U is the depth-averaged, time-varying horizontal fluid velocity within the canopy. The force predicted by Eqs. (4) and (5) was validated with measured force in pure waves [25].

An adaptation of Eqs. (4) and (5) was considered here for marsh plants exposed to combined waves and current such that velocity defining the plant force is

$$U(t) = \alpha_c U_c + \alpha_w U_w \cos(\omega t), \quad (6)$$

in which α_c and α_w are coefficients representing the impact of meadow on the in-canopy time-mean current ($\alpha_c U_c$) and the in-canopy wave orbital velocity ($\alpha_w U_w$), in comparison to the depth average current U_c (defined over h) and wave velocity U_w [defined over $h_p = \min(h, l_s + l_l)$] unaffected by the plants, respectively (Fig. 1). Based on linear-wave theory

$$U_w = \frac{1}{h_p} \int_0^{h_p} a_w \omega \frac{\cosh kz}{\sinh kh} dz, \quad (7)$$

in which k is the wave number.

Within a submerged canopy, the time-mean current [39,40] and wave orbital velocity [41,42] can be reduced by canopy drag, i.e., $\alpha_c < 1$ and $\alpha_w < 1$, respectively (Fig. 1). Experimental measurements suggest that α_c and α_w are not codependent [41], so that α_c and α_w can be predicted

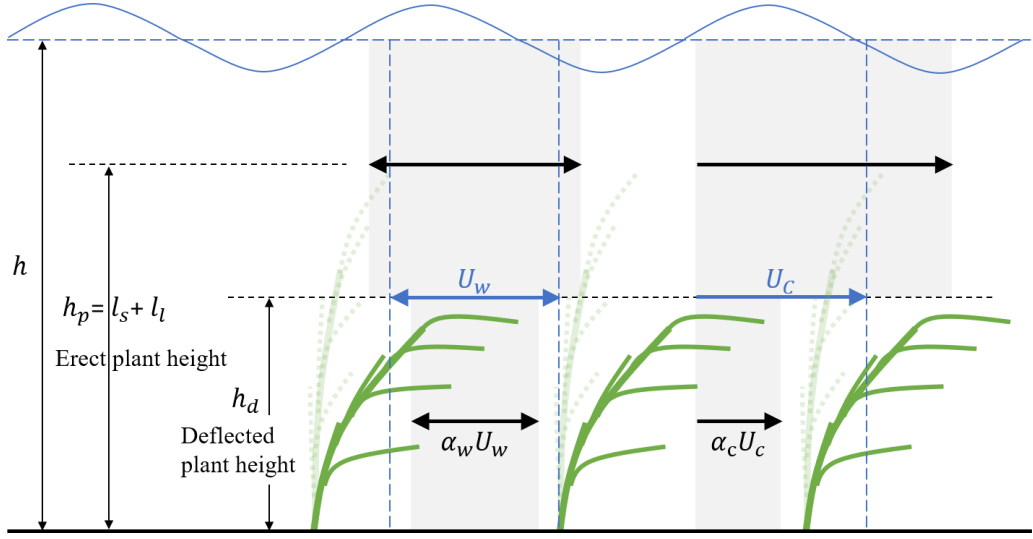


FIG. 1. Light and dark green plants represent positions at trough and crest, respectively. Due to canopy resistance, in-canopy time-mean current ($\alpha_c U_c$) and wave orbital velocity ($\alpha_w U_w$) are reduced compared to imposed current (U_c , defined over h) and wave orbital velocity [U_w , defined over the erect plant height h_p , Eq. (7)]. The reduction in canopy height (h_d) due to reconfiguration feeds back to $\alpha_c U_c$ and $\alpha_w U_w$ by changing the in-canopy solid volume fraction and plant force per unit volume of in-canopy fluid.

separately. Specifically, α_c can be predicted by solving Eqs. (18) to (20) in Ref. [39] with the plant force predicted by Eq. (4). α_w can be predicted by solving the 2-box momentum model (Eq. (1.3) in Ref. [42]). Due to reconfiguration, the canopy height represented by the time-mean plant height, h_d , is a function of in-canopy current $\alpha_c U_c$, which in turn modifies α_c and α_w (Fig. 1). Consequently, h_d and α_c must be predicted iteratively with h_d estimated using Eq. (4) in Ref. [43], which was used to predict α_w . The details of in-canopy velocity prediction are described in the Supplemental Material [44].

Finally, the maximum fluid velocity in the canopy,

$$U_{\max} = \alpha_c |U_c| + \alpha_w U_w, \quad (8)$$

was used to define Ca_l and Ca_s in Eq. (4), and to define the drag and inertial coefficients in Eq. (5) from their measured dependence on Keulegan and Carpenter number (KC) [45], following Fig. 1 in Ref. [46], but with KC defined using U_{\max} ($KC_l = U_{\max} T_w / b$ for a flat leaf and $KC_s = U_{\max} T_w / D$ for a circular stem, with T_w the wave period). Supporting this, a previous study showed that drag coefficients for combined waves and current followed the same dependence as pure waves, with KC defined by the maximum horizontal velocity [47]. The modified version of Eqs. (4) and (5) for combined waves and current was validated using force measurements on a single plant [48]. An example is included in the Supplemental Material [44].

B. Wave dissipation

Assuming no interaction between plants, the force on an individual plant [Eqs. (4) to (8)] can be used to estimate the energy dissipation within a meadow of N_s plants per bed area. If energy dissipation is due only to the work done by the force on the plant, F_d , the rate of energy dissipation is [49]

$$E_D = E_{\text{plant}} = \frac{1}{T_w} \int_{t=0}^{T_w} N_s F_d U dt. \quad (9)$$

The total dissipation rate E_D can be divided into wave energy dissipation, $E_{D,w}$, and current dissipation, $E_{D,c}$. Following Refs. [29,30], the current energy dissipation can be estimated from the in-canopy, time-mean velocity U_m ($=\alpha_c U_c$) and current-induced force,

$$E_{D,c} = N_s F_c U_m. \quad (10)$$

The current-induced force within the canopy, F_c , was estimated assuming that the time-average drag coefficient for a flexible meadow could be inferred from the predicted maximum force and maximum velocity, $|F_d|_{\max}/U_{\max}^2$,

$$|F_c| = \frac{|F_d|_{\max}}{U_{\max}^2} U_m^2. \quad (11)$$

The wave energy dissipation is then

$$E_{D,w} = E_D - E_{D,c} = -C_g \frac{\partial(\frac{1}{2} \rho g a_w^2)}{\partial x}, \quad (12)$$

in which C_g is the wave group velocity, which can be modified by the current due to the Doppler effect [33],

$$C_g = C_{g,cw} = U_c + C_{g,pw} = U_c + \frac{1}{2} \left(1 + \frac{2kh}{\sinh(2kh)} \right) \left[\frac{g}{k} \tanh(kh) \right]^{1/2}. \quad (13)$$

The subscripts *cw* and *pw* indicate combined current-wave conditions and pure wave conditions, respectively. Note that Eqs. (10) to (12) assume that nonlinear terms arising between the wave and current contribute to wave dissipation. Using Eq. (12), the decay of wave amplitude along the meadow can be estimated progressively using step length dx ,

$$a_{w,ndx} = \sqrt{a_{w,(n-1)dx}^2 - \frac{E_{D,w} dx}{1/2 \rho g C_g}}, \quad (14)$$

in which $a_{w,ndx}$ is the wave amplitude at $x = ndx$ from the meadow edge in the direction of wave propagation. Starting from the wave amplitude $a_{w,0}$ at the marsh edge ($x = 0$), the wave amplitude ($a_{w,x}$) at each location $x = ndx$, $n = 1 : N$, was estimated by marching through the following steps. Equation (4) predicted $F_d(t)$, which was used in Eqs. (9) to (12) to obtain the wave energy dissipation rate, $E_{D,w}$, which was used in Eq. (14) to predict the wave amplitude at the next position in the meadow, $a_{w,ndx}$. The step size dx was decreased until its value had no impact on the solution, which was satisfied by $dx = 0.1$ m ($\ll 1/5$ wavelength).

To facilitate comparison amongst many cases, the amplitude decay was converted to a coefficient of spatial wave decay, K_D , as defined in Ref. [50],

$$\frac{a_{w,x}}{a_{w,0}} = \frac{1}{1 + K_D a_{w,0} x}. \quad (15)$$

Specifically,

$$K_D = \frac{1}{Ndx} \left(\frac{1}{a_{w,ndx}} - \frac{1}{a_{w,0}} \right), \quad (16)$$

with $a_{w,0}$ and $a_{w,x}$ the wave amplitude measured at the leading edge of the meadow and at distance x from the leading edge, respectively.

The predicted wave dissipation was validated against measurements in a meadow of model plants; see Sec. IV B. After validation, the model was used to explore a wider range of conditions, including both following and opposing current with $U_c/U_w = -5$ to 5 and for varying plant flexibility and plant morphology; see Sec. V. Predicted K_D shown in Sec. V were evaluated over a distance of one wavelength for meadow density $N_s = 280$ plants/m², with an erect height of

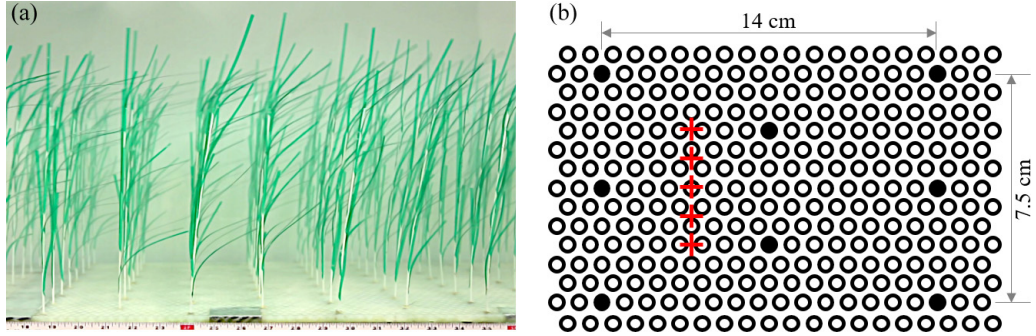


FIG. 2. (a) Model *Spartina alterniflora*. (b) Arrangement of plants (filled circles) within the staggered baseboard holes (open circles). Red plus signs are the locations of velocity profiles inside the meadow.

0.6 m in water depth $h = 1$ m. The wave amplitude $a_{w,0} = 0.1$ m, and wave period $T_w = 2$ s, which correspond to $U_w = 22.5$ cm/s and wavelength = 5.2 m, were kept constants.

III. EXPERIMENTAL MEASUREMENTS

Model plants were constructed with ten leaves (10 cm long, 3 mm wide, and 0.12 mm thick) and a central stem [20 cm long and 2 mm diameter, Fig. 2(a)]. The model plants are geometrically (1:5) and dynamically similar to *Spartina alterniflora* [17]. The material density and the elastic modulus were 1.35 g/cm³ and 4.8 GPa for the leaf, and 1.06 g/cm³ and 1.72 GPa for the stem, respectively [25]. The plants were arranged in a staggered pattern [Fig. 2(b)] to construct a 3.8-m-long meadow with shoot density of $N_s = 280$ plants/m² and a fully erect height of 30 cm.

The meadow was installed in a recirculating flume that is 24 m long and 38 cm wide (Fig. 3). A beach with 1:5 slope and covered with 10-cm-thick coconut fiber mats reduced wave reflection to $7 \pm 3\%$. To allow the current to pass, two wooden bricks elevated the toe of the beach 9 cm above the bed. Three water depths (18, 27, and 40 cm) produced emergent and submerged conditions. Four wave amplitudes and two current velocities were tested (Table II). The current and wave conditions were chosen to cover a range of Cauchy number Ca and length ratio L observed in the field. Dynamic

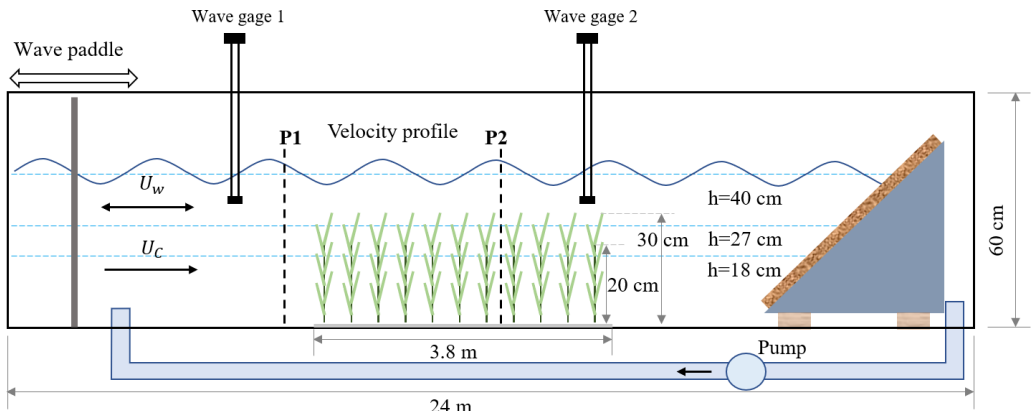


FIG. 3. Schematic of experiment setup, not to scale. The wave paddle and current inlet are located at the left and the beach to the right. Free-surface displacement was simultaneously measured at a fixed position (wave gage 1) and multiple positions along the meadow (wave gage 2). A Nortek Vectrino+ measured velocity profiles 2 m upstream of the meadow (P1) and one wavelength into meadow (P2).

TABLE II. Experimental conditions: current (U_c), wave amplitude (a_w), water depth (h), and wave orbital velocity, U_w . The wave frequency was 0.7 Hz. Pure wave and pure current cases given with notation Wi (i th wave condition) and Cj (j th current condition), respectively. Combined cases given with notation $WiCj$ through the paper.

| Current case | $U_c \pm 0.4$ cm/s | Wave case | h (cm) | $a_w \pm 0.1$ cm/s | $U_w \pm 1$ cm/s |
|--------------|--------------------|-----------|----------|--------------------|------------------|
| C1 | 4.7 | W1 | 18 | 1.0 | 6 |
| C2 | 7.8 | W2 | 18 | 2.2 | 15 |
| | | W3 | 27 | 1.0 | 5.5 |
| | | W4 | 27 | 2.2 | 11 |
| | | W5 | 27 | 3.2 | 15 |
| | | W6 | 40 | 2.2 | 9 |
| | | W7 | 40 | 3.2 | 13 |
| | | W8 | 40 | 4.0 | 16 |

similarity was achieved by matching Ca (ratio of hydrodynamic force to plant restoring force due to rigidity). Similarly, the kinematic similarity was achieved by matching L (ratio of plant element length to wave orbital excursion). The wave decay over the meadow was measured for both pure waves (8 cases) and waves with current (16 cases). Parameters for each case are summarized in Table S1 in the Supplemental Material [44].

Two wave gages were synchronized to measure the free-surface displacement at a reference position 4 m upstream of the meadow (wave gage 1) and at a mobile position along the meadow (wave gage 2). During each experiment (about 90 min), the wave amplitude at wave gage 1 varied by less than 3%, confirming stationary wave conditions. The wave amplitude measured by wave gage 1 is listed in Table II. Wave gage 2 collected data at 10-cm intervals along the meadow. At each position, free-surface displacement, $\eta(t)$, was recorded at 2000 Hz for 1 min. Additional measurements of wave amplitude were made without plants to assess wave decay associated with the channel wall and baseboard alone. The phase-averaged surface displacement, $\hat{\eta}$, was determined following the method in Ref. [25]. The wave amplitude a_w was calculated from the root-mean-square of phase-averaged surface displacement, $a_w = \sqrt{2} \hat{\eta}_{\text{rms}}$.

The spatial evolution of wave amplitude reflected the sum of the incoming wave and the beach-reflected wave, resulting in an amplitude modulation at an interval of $\lambda/2$ (with wavelength λ , e.g., Fig. 4). Solving Eq. (15) for $a_{w,x}$ and accounting for the wave modulation, the wave decay coefficient K_D was estimated by fitting the measured amplitude to the following [21]:

$$\frac{1}{a_{w,x}} = K_D x + C_1 \cos(2kx + \epsilon) + C_2, \quad (17)$$

in which $k = 2\pi/\lambda$ is the wave number, and ϵ , C_1 , and C_2 are fitting parameters. Examples are shown in Fig. 4. Wave amplitudes along the meadow were summarized in Table S3 in Supplemental Material [44]. Wave decay attributed to plants (K_D , Table S1 in Supplemental Material [44]) was obtained by subtracting the decay coefficient obtained in the flume without plants.

Nortek Vectrino+ was used to measure vertical profiles of velocity with 1- to 2-cm vertical resolution at 2 m in front of and one wavelength inside the meadow (Fig. 3). In front of the meadow velocity was measured at the flume centerline. Inside the meadow velocity was measured at five lateral locations to capture plant-scale heterogeneity [red pluses in Fig. 2(b)]. At each measurement point, the Vectrino+ recorded a 1-min record at 200 Hz. Each velocity record was separated into phase bins, despiked within each phase bin using the methods described in Refs. [51,52], and quality checked by the signal to noise ratio. The velocity within each phase-bin was averaged to produce the phase-averaged velocity $\langle u \rangle(\phi)$, which contained both wave and current components. The time-mean

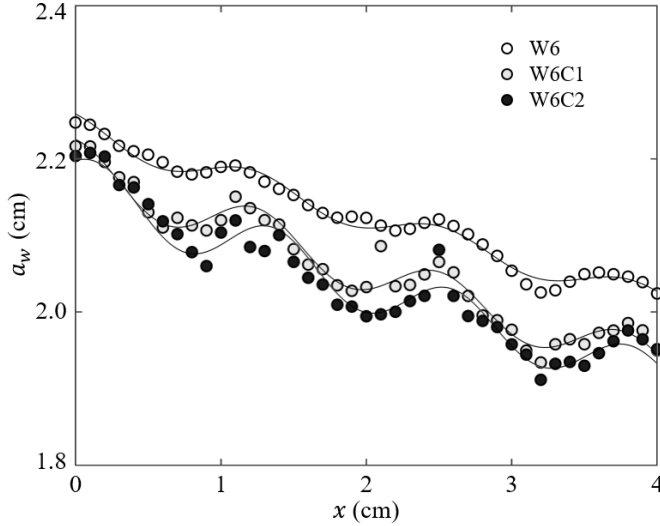


FIG. 4. Measured wave amplitude (symbols) starting from meadow leading edge ($x = 0$) and Eq. (17) (curves) for W6 (pure wave), W6C1 (wave 6+current 1), and W6C2 (wave 6+current 2). Based on fitted Eq. (17), $K_D = 1.24 \pm 0.05$, 1.51 ± 0.08 , and $1.52 \pm 0.11 \text{ m}^{-2}$ with 95% CI, respectively.

velocity u_m was defined as the average of $\langle u \rangle(\phi)$,

$$u_m = \frac{1}{2\pi} \int_0^{2\pi} \langle u \rangle(\phi) d\phi. \quad (18)$$

The phase-averaged wave velocity $\langle u_w \rangle(\phi) = \langle u \rangle(\phi) - u_m$, from which the magnitude of wave orbital velocity was estimated as

$$u_w = \sqrt{2 \frac{1}{2\pi} \int_0^{2\pi} [\langle u_w \rangle(\phi)]^2 d\phi}. \quad (19)$$

The vertical average within the canopy of the time-mean and wave orbital velocity were denoted by U_m and U_w , respectively. For submerged conditions, velocity was measured over the entire plant height, and U_m was the depth-averaged time-mean velocity over h_p at P2. For emergent conditions, the Vectrino could not measure the uppermost 5 cm of canopy. Since the canopy solid volume fraction was small, U_m at P1 and P2 were essentially the same for emergent cases, such that U_m was estimated at P1, which had a more uniform velocity profile (compared to P2). Finally, for comparison, the velocity was also measured under pure current, for which u_m was defined with time average only. For pure current, the time-mean, depth-averaged velocity over the water depth at P1 (2 m upstream of the canopy) defined the imposed current, U_c . When waves were present, U_m was smaller than U_c (Table II) by an amount that equals the Stokes drift [53].

IV. EXPERIMENTAL RESULTS AND MODEL VALIDATION

A. Flow structure

Because wave dissipation will depend on the velocity within the canopy, we must first understand how the canopy drag influences the current and wave velocity structure. Comparing to the profiles measured in the bare channel upstream of the meadow (black symbols in Fig. 5), the meadow modified the time-mean velocity, but had little influence on the wave orbital velocity (red symbols

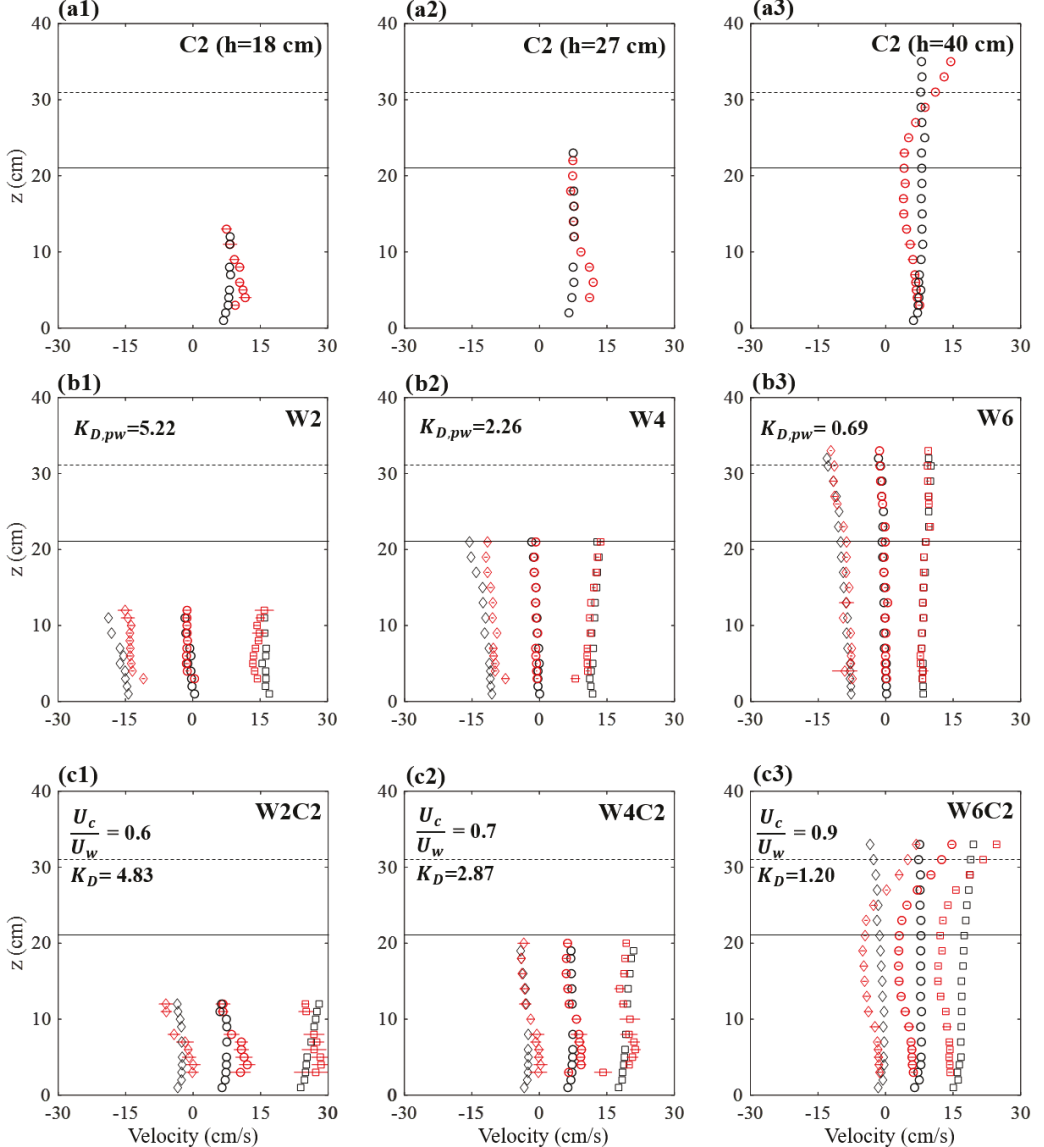


FIG. 5. The measured velocity for (a) pure current ($C2, U_c = 7.8 \text{ cm/s}$), (b) pure wave ($a_w = 2.2 \text{ cm}$), and (c) combined current and waves ($U_c = 7.8 \text{ cm/s}, a_w = 2.2 \text{ cm}$), with each column a different water depth, $h = 18, 27$, and 40 cm from left to right. The corresponding case names were shown on the top right of each subplot. Black symbols denote profile P1 (2 m in front of the meadow) and red symbols denote the average of five measurements at P2 [Fig. 2(b)], with horizontal bar indicating standard deviation of the five values. Circles are time-mean velocity. Squares and diamonds denote maximum and minimum velocity over the wave period, when waves were present. The horizontal solid and dashed lines indicate erect stem height and full plant height, h_p . For the cases considered, the deflected canopy height $h_d \approx h_p$.

in Fig. 5). First, under pure current (top row in Fig. 5), the velocity in the meadow was increased near the bed $z < 12 \text{ cm}$, where the frontal area was smaller. An inverse relation between velocity and frontal area has also been reported in previous studies [54–56]. When the plants were submerged, the in-canopy velocity (red circles) was reduced, compared to the bare channel (black circles), because

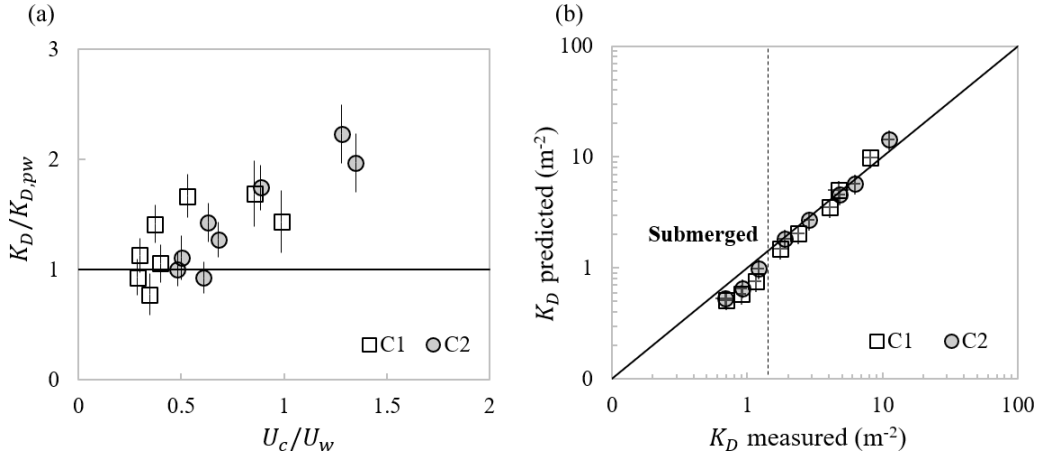


FIG. 6. (a) The ratio of wave decay coefficient in combined currents and waves, K_D , to that in pure waves, $K_{D,pw}$ plotted against U_c/U_w . (b) The predicted vs the measured wave decay coefficient K_D . Measured error indicates 95% CI for fitting method [Eq. (17)]. Predictions were estimated to have 20% uncertainty. The vertical line separates the submerged (left) to near-emergent and emergent conditions (right).

flow was diverted above the meadow [Fig. 5(a3)]. This shape of velocity profile has also been observed in many previous papers, including submerged live *Eurasian watermilfoil* by Lopez [57] (see Fig. 1.1 in their paper).

Second, for pure waves the in-canopy velocity (red symbols) was similar to that measured in front of the meadow (black symbols), and both were consistent with linear wave theory [Fig. 5(b)]. Wave dissipation by the meadow resulted in slightly smaller wave velocity at P2 compared to P1.

Third, for combined waves and current, the shape of the time-mean profile was similar to that observed for pure current [circles in Figs. 5(a) and 5(c)]. Specifically, the near-bed velocity was higher than the mean in-canopy velocity, and, for the submerged canopy, a shear layer was formed starting at the top of the stem height (solid horizontal line). When the time-mean velocity was subtracted, the remaining velocity was consistent with the pure wave profile (linear wave profile), illustrating that the canopy modified the vertical distribution of time-mean current velocity, but had little impact on the wave orbital velocity. This was consistent with Lowe *et al.* [41], who described how plants are more efficient at attenuating current than waves with short wave orbital excursion. This observation also supports the assumption that waves did not significantly alter the momentum balance of the time-mean current, consistent with Eqs. (11) and (12). A summary of velocity measurements at P1 and P2 for all cases are listed in Table S2 in the Supplemental Material [44].

B. Wave decay by marsh plants and model validation

As a general trend, and specifically for $U_c/U_w > 0.6$, the measured wave decay increased as U_c/U_w increased. However, for some small currents, the wave decay coefficient for combined current and waves, K_D , was decreased compared to that for pure waves $K_{D,pw}$ [Fig. 6(a)]. One example was shown in Fig. 5(c), in which U_c/U_w increased from 0.6 to 0.9, and the associated wave decay increased from $K_D/K_{D,pw} = 0.9$ to 1.7. The decrease in wave dissipation was most apparent for the weaker current (squares in Fig. 6). A similar transition was observed for rigid canopies [29–31]. Specifically, $K_D/K_{D,pw} < 1$ for U_c/U_w smaller than a transition value of 0.65 to 1.25 [29] and 0.37 to 1.54 [31], but increased above pure wave ($K_D/K_{D,pw} > 1$) for higher following currents [29–31].

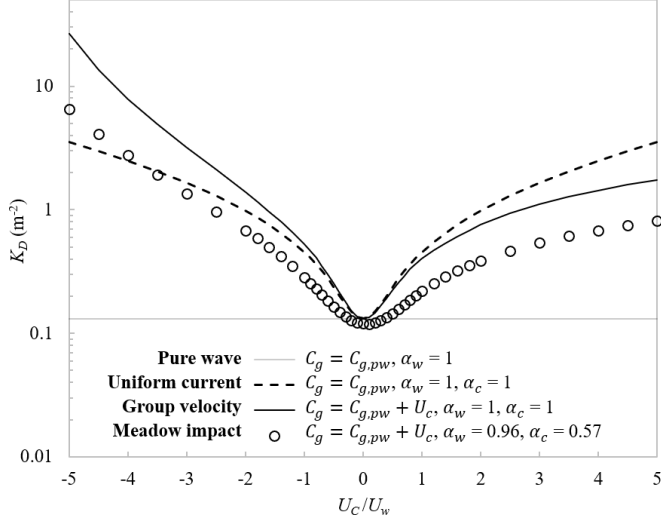


FIG. 7. Wave decay coefficient K_D vs velocity ratio for a meadow of rigid stems ($l_s = 0.6$ m, $D = 5$ mm, and $N_s = 280$ stems/m², $h = 1$ m, $a_w = 0.1$ m, and $T_w = 2$ s). The different curves (see legend) consider different mechanisms that influence wave dissipation.

The decay coefficient was predicted using Eqs. (10) to (16), as described in Sec. II and using the measured U_m and linear wave orbital velocity within the canopy, i.e., $\alpha_w = 1$. The predicted wave decay coefficients agreed with the measured values to within $17 \pm 12\% (\pm \text{SD})$, with $K_D(\text{predicted}) = (1.06 \pm 0.08)K_D(\text{measured})$ [Fig. 6(b)]. The measured wave decay coefficients are summarized in Table S1 in the Supplemental Material [44]. The model worked well for the emergent and near-emergent cases, but underpredicted the submerged cases [to the left of the vertical line in Fig. 6(b)]. This can be explained by a difference in the degree of vertical flow adjustment due to the canopy. For emergent cases there is little vertical flow adjustment [Figs. 5(a1) and 5(c1)], so that the in-canopy velocity profile can be established close to the leading edge and the vertically averaged U_m is representative of the current over the entire canopy height and length. However, for submerged cases, there is significant flow adjustment [Figs. 5(a3) and 5(c3)] as the in-canopy velocity decreases and above-canopy velocity increases over an adjustment length scale proportional to the canopy height [39]. Consequently, for the submerged meadow, the measured U_m at $x = 2.4$ m (one wavelength) underestimates the velocity near the leading edge. In addition, because of the shear layer at the top of the submerged meadow [Figs. 5(a3) and 5(c3)], U_m underestimates the velocity in the upper canopy. The underestimation of in-canopy velocity could explain the underprediction of K_D .

V. MODEL EXPLORATION TO ILLUSTRATE MECHANISMS IMPACTING WAVE DISSIPATION BY VEGETATION

A. Impact of current

To illustrate the different mechanisms impacting wave dissipation by vegetation, we first consider a meadow of rigid cylindrical stems with diameter $D = 5$ mm. For pure waves, the predicted $K_D = 0.13$ m⁻², which is included as a gray horizontal reference line in Fig. 7. First, consider the impact of a vertically uniform current of magnitude U_c (denoted “uniform current,” dashed curve in Fig. 7). For this case $C_g = C_{g,pw}$, $\alpha_w = 1$, and $\alpha_c = 1$. With the uniform current, the wave dissipation increased symmetrically with increasing current magnitude $|U_c|$ for both opposing and following current. This makes sense, because adding current increased the total fluid velocity and

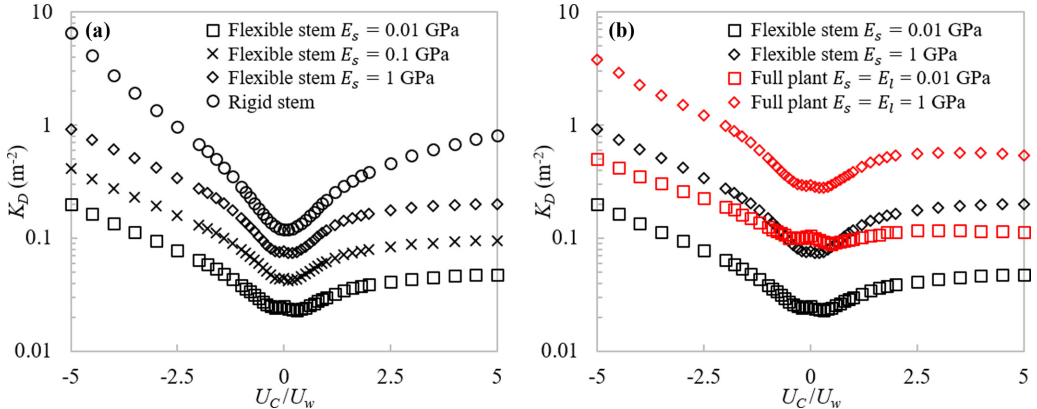


FIG. 8. Wave decay coefficient vs velocity ratio for (a) meadow of stems with different stem rigidity, and (b) plants with and without leaves. $N_s = 280 \text{ stems/m}^2$, $l_s = 0.6 \text{ m}$, and $D = 5 \text{ mm}$ with elastic modulus given in legend. Wave conditions were constant ($h = 1 \text{ m}$, $a_w = 0.1 \text{ m}$, and $T_w = 2 \text{ s}$). Full plants have $N_l = 10$ leaves each $l_l = 0.3 \text{ m}$ long, $b = 10 \text{ mm}$ width, and, $d = 0.3 \text{ mm}$ thick.

thus plant force, resulting in a greater wave energy dissipation. Specifically, the wave dissipation with current, $E_{D,w} = E_D - E_{D,c} \sim |U_{\max}^3| - |U_c^3| = |U_w^3| + 3U_w^2|U_c| + 3U_wU_c^2$ [Eqs. (9) to (12)], was always greater than energy dissipation for the same pure wave $E_{D,w} \sim |U_w^3|$.

Second, additionally consider the impact of current on the group velocity (denoted “group velocity,” solid curve in Fig. 7). For this case, the group velocity $C_g = C_{g,pw} + U_c$ [Eq. (13)], $\alpha_w = 1$, and $\alpha_c = 1$, in comparison to uniform current case ($C_g = C_{g,pw}$, $\alpha_w = 1$, and $\alpha_c = 1$). The increase in K_D is now greater for an opposing current of the same magnitude. As illustrated in Eq. (12), the group velocity, C_g , connects the time rate of wave energy dissipation ($E_{D,w}$) to the spatial rate of wave energy dissipation [represented by K_D , Eq. (15)]. For the same $|U_c|$ (associated with the same $E_{D,w}$), an opposing (following) current decreases (increases) C_g [Eq. (13)] and generates larger (smaller) K_D (spatial rate of amplitude decay), which is shown by the asymmetric black curve in Fig. 7. A larger K_D for an opposing current, compared to a following current, has been measured in meadows of rigid cylinders [31] and live *Puccinellia maritima* and *Spartina anglica* [32–34]; however, the role of group velocity was not previously identified.

Finally, additionally consider the impact of the meadow drag in reducing the in-canopy velocity magnitude (denoted “meadow impact,” circles in Fig. 7). The reduction of in-canopy time-mean and wave velocity due to plant drag (Fig. 1) can both reduce the wave decay. For the conditions considered, $\alpha_w = 0.96$ and $\alpha_c = 0.57$, which reduced K_D (circles) compared to the prediction made without considering the reduction of current within the meadow ($\alpha_c = 1$, solid curve), which highlighted the importance of considering the in-canopy velocity. Note that the meadow is more efficient in dissipating current than waves [41], with $\alpha_c \ll 1$ but $\alpha_w \approx 1$.

B. Impact of flexibility

Continuing with the meadow of cylindrical stems, we next considered the impact of flexibility by varying the modulus $E_s = 0.01$ to 1 GPa [Fig. 8(a)], with the lowest value based on live *Puccinellia maritima* ($E_s = 0.013 \text{ GPa}$ from Ref. [33]) and the upper value chosen to approach rigid behavior. Wave dissipation decreased with decreasing stem rigidity (decreasing E_s), and this was explained primarily by the reduction in plant force due to reconfiguration. Specifically, for each tenfold decrease in E_s , C_{a_s} increased tenfold, which decreased the force by the reconfiguration factor $(C_{a_s}L_s)^{-1/4}$ [see Eq. (4)], i.e., by $10^{-1/4} = 0.56$. Consistent with this, the curves of K_D for $E_s = 1$, 0.1 , and 0.01 GPa sequentially decreased in magnitude by factors of 0.45 to 0.58 . Small deviations from the reconfiguration scaling (0.56) were due to coincident changes in the in-canopy velocity.

Specifically, $\alpha_c = 0.53$ to 0.73 and $\alpha_w = 0.86$ to 0.99 across the different current and stem rigidity (see Fig. A1 in the Supplemental Material [44]).

C. Impact of leaves

A full plant morphology was constructed by adding $N_l = 10$ leaves to each stem, each with length $l_l = 0.3$ m, width $b = 10$ mm, and thickness $d = 0.3$ mm. With the addition of leaves [red symbols in Fig. 8(b)] K_D increased by a factor of 2.4 to 4.2 compared to stems alone (black symbols) with the same elastic modulus. This highlighted the important role of leaves in wave dissipation, although they are typically neglected in coastal models [49,50]. The leaves increased the plant force by 3.8 to 4.3 times the force on the stem alone for the same in-canopy velocity, which increased wave dissipation [Eq. (12)]. However, the changes in K_D (2.4 to 4.2) were smaller than the changes in force ratio (3.8 to 4.3), because the increased force also lowered the in-canopy velocity ratio ($\alpha_c = 0.36$ to 0.59 and $\alpha_w = 0.75$ to 0.98 , Fig. A1 in Supplemental Material [44]), which mitigated the increase in wave dissipation. For the most flexible plant considered ($E_s = 0.01$, red squares), K_D was relatively insensitive to the addition of a following current, a result that was quite different from the original rigid model [circle in Fig. 8(a)]. This arose from the competing effects of the current influencing the group velocity [Eq. (13)] and in-canopy velocity reduction, which was impacted by the deflected canopy height. The interplay of these effects is discussed in the next section.

D. Reduction in K_D for small current

In some cases, the addition of a weak current reduced K_D . For the most flexible plant [red squares in Fig. 8(b)] $K_D/K_{D,pw} < 1$ for $-0.5 \leq U_c/U_w \leq 1.4$. A reduction in wave dissipation due to small following currents has also been observed for flexible model plants [35] and live plants [32–34]. Previous studies attributed the reduction to plant deflection [35]. Here, a more comprehensive explanation can be provided, based on changes in group velocity and in-canopy time-mean and wave orbital velocity. First, as noted in the previous sections, a following current increased the group velocity, which decreased K_D . Second, due to the plant reconfiguration, a following current decreased the deflected canopy height, h_d , such that plant force was distributed over a smaller canopy volume, which reduced in-canopy velocity (reduced α_c and α_w ; see Fig. A1 in the Supplemental Material [44]). Because U_w was constant across cases, the in-canopy orbital velocity ($\alpha_w U_w$) decreased with increasing $|U_c|$, which tended to decrease K_D . Finally, even though α_c decreased, the in-canopy time mean $|U_m|$ ($= \alpha_c |U_c|$) increased with $|U_c|$, which increased wave dissipation $E_{D,w}$ [Eqs. (11) to (13)]. For a following current, the decreasing trend in K_D due to decreasing in-canopy wave velocity and increasing wave group velocity counteracted the increasing trend due to increasing $|U_m|$. For the full plant [red squares in Fig. 8(b)], this interplay resulted in a K_D that, for small $|U_m|$, was reduced relative to pure wave. This also explained the observations in previous studies of flexible live and model plants [29,31,33,35]. Further, due to reconfiguration and leaves, K_D was less sensitive to the addition of large current, compared to the rigid model [circles in Fig. 8(a)] considered by previous studies.

VI. CONCLUSION

A model was developed to capture the influence of plant flexibility, leaves, and current on wave dissipation by a meadow of marsh plants. The model was validated by wave decay measured over a meadow of flexible model plants geometrically similar to *Spartina alterniflora*. Importantly, the canopy drag changed the time-mean velocity profile for both pure current and combined current and wave conditions, and the adjusted in-canopy velocity was needed to achieve correct prediction of wave dissipation. Current was shown to impact wave dissipation through two mechanisms. First, the addition of a time-mean velocity within the canopy enhanced the force exerted on the plants, which results in an increase in the wave energy dissipation. Second, the addition of current modified the wave group velocity, which tended to increase spatial wave decay in opposing current, but

to decrease it in following current. Importantly, for real plant morphology and flexibility K_D was significantly less sensitive to the addition of current, compared to the rigid plants, because the reconfiguration of the meadow and the drag associated with the leaves tended to reduce the wave and current velocity within the meadow, which mitigated the impact of current on wave dissipation.

ACKNOWLEDGMENTS

X.Z. was supported by the China Scholarship Council. The project also received support from the U.S. National Science Foundation under Grant No. EAR-1659923. Any opinions, findings, and conclusions in this paper are those of the author(s) and do not necessarily reflect the views of the China Scholarship Council or the U.S. National Science Foundation.

- [1] I. Moeller, T. Spencer, and J. R. French, Wind wave attenuation over saltmarsh surfaces: Preliminary results from Norfolk, England, *J. Coastal Res.* **12**, 1009 (1996).
- [2] F. Rupprecht, I. Möller, M. Paul, M. Kudella, T. Spencer, B. K. van Wesenbeeck, G. Wolters, K. Jensen, T. J. Bouma, M. Miranda-Lange, and S. Schimmele, Vegetation-wave interactions in salt marshes under storm surge conditions, *Ecol. Eng.* **100**, 301 (2017).
- [3] T. Ysebaert, S. Yang, L. Zhang, Q. He, T. J. Bouma, and P. M. J. Herman, Wave attenuation by two contrasting ecosystem engineering salt marsh macrophytes in the intertidal pioneer zone, *Wetlands* **31**, 1043 (2011).
- [4] J. Carus, M. Paul, and B. Schröder, Vegetation as self-adaptive coastal protection: Reduction of current velocity and morphologic plasticity of a brackish marsh pioneer, *Ecol. Evol.* **6**, 1579 (2016).
- [5] H. M. Nepf, Drag, turbulence, and diffusion in flow through emergent vegetation, *Water Resour. Res.* **35**, 479 (1999).
- [6] Z. Zhu, V. Vuik, P. J. Visser, T. Soens, B. van Wesenbeeck, J. van de Koppel, S. N. Jonkman, S. Temmerman, and T. J. Bouma, Historic storms and the hidden value of coastal wetlands for nature-based flood defence, *Nat. Sustainability* **3**, 853 (2020).
- [7] S. Narayan, M. W. Beck, P. Wilson, C. J. Thomas, A. Guerrero, C. C. Shepard, B. G. Reguero, G. Franco, J. C. Ingram, and D. Trespalacios, The value of coastal wetlands for flood damage reduction in the northeastern USA, *Sci. Rep.* **7**, 9463 (2017).
- [8] K. Schoutens, M. Heuner, V. Minden, T. Schulte Ostermann, A. Silinski, J.-P. Belliard, and S. Temmerman, How effective are tidal marshes as nature-based shoreline protection throughout seasons, *Limnol. Oceanogr.* **64**, 1750 (2019).
- [9] K. Elschot, T. J. Bouma, S. Temmerman, and J. P. Bakker, Effects of long-term grazing on sediment deposition and salt-marsh accretion rates, *Estuarine Coastal Shelf Sci.* **133**, 109 (2013).
- [10] A. E. Sutton-Grier, K. Wowk, and H. Bamford, Future of our coasts: The potential for natural and hybrid infrastructure to enhance the resilience of our coastal communities, economies and ecosystems, *Environ. Sci. Policy* **51**, 137 (2015).
- [11] C. M. Duarte, I. J. Losada, I. E. Hendriks, I. Mazarrasa, and N. Marbà, The role of coastal plant communities for climate change mitigation and adaptation, *Nat. Clim. Change* **3**, 961 (2013).
- [12] K. B. Gedan, M. L. Kirwan, E. Wolanski, E. B. Barbier, and B. R. Silliman, The present and future role of coastal wetland vegetation in protecting shorelines: Answering recent challenges to the paradigm, *Clim. Change* **106**, 7 (2011).
- [13] K. Schoutens, M. Heuner, E. Fuchs, V. Minden, T. Schulte-Ostermann, J.-P. Belliard, T. J. Bouma, and S. Temmerman, Nature-based shoreline protection by tidal marsh plants depends on trade-offs between avoidance and attenuation of hydrodynamic forces, *Estuarine Coastal Shelf Sci.* **236**, 106645 (2020).
- [14] K. K. Arkema, R. Griffin, S. Maldonado, J. Silver, J. Suckale, and A. D. Guerry, Linking social, ecological, and physical science to advance natural and nature-based protection for coastal communities, *Ann. N.Y. Acad. Sci.* **1399**, 5 (2017).

[15] M. E. Anderson and J. M. Smith, Wave attenuation by flexible, idealized salt marsh vegetation, *Coastal Eng.* **83**, 82 (2014).

[16] R. Jadhav and Q. Chen, Field investigation of wave dissipation over salt marsh vegetation during tropical cyclone, *Coastal Eng.* **1**, 41 (2012).

[17] X. Zhang, P. Lin, Z. Gong, B. Li, and X. Chen, Wave attenuation by spartina alterniflora under macro-tidal and storm surge conditions, *Wetlands* **40**, 2151 (2020).

[18] F. P. Gosselin, Mechanics of a plant in fluid flow, *J. Exp. Bot.* **70**, 3533 (2019).

[19] M. Luhar and H. M. Nepf, Wave induced dynamics of flexible blades, *J. Fluids Struct.* **61**, 20 (2016).

[20] T. J. van Veelen, T. P. Fairchild, D. E. Reeve, and H. Karunarathna, Experimental study on vegetation flexibility as control parameter for wave damping and velocity structure, *Coastal Eng.* **157**, 103648 (2020).

[21] J. Lei and H. Nepf, Wave damping by flexible vegetation: Connecting individual blade dynamics to the meadow scale, *Coastal Eng.* **147**, 138 (2019).

[22] J. C. Mularney and S. M. Henderson, Wave-forced motion of submerged single-stem vegetation, *J. Geophys. Res.* **115**, C12061 (2010).

[23] S. M. Henderson, Motion of buoyant, flexible aquatic vegetation under waves: Simple theoretical models and parameterization of wave dissipation, *Coastal Eng.* **152**, 103497 (2019).

[24] M. Abdolahpour, M. Ghisalberti, K. McMahon, and P. S. Lavery, The impact of flexibility on flow, turbulence, and vertical mixing in coastal canopies, *Limnol. Oceanogr.* **63**, 2777 (2018).

[25] X. Zhang and H. Nepf, Wave-induced reconfiguration of and drag on marsh plants, *J. Fluids Struct.* **100**, 103192 (2021).

[26] M. Heuner, A. Silinski, J. Schoelynck, T. J. Bouma, S. Puijalon, P. Troch, E. Fuchs, B. Schröder, U. Schröder, P. Meire, and S. Temmerman, Ecosystem engineering by plants on wave-exposed intertidal flats is governed by relationships between effect and response traits, *PLoS One* **10**, e0138086 (2015).

[27] R. O. Tinoco, J. E. San Juan, and J. C. Mularney, Simplification bias: Lessons from laboratory and field experiments on flow through aquatic vegetation, *Earth Surf. Process. Landforms* **45**, 121 (2020).

[28] H. Cao, Z. Zhu, R. James, P. M. J. Herman, L. Zhang, L. Yuan, and T. J. Bouma, Wave effects on seedling establishment of three pioneer marsh species: Survival, morphology and biomechanics, *Ann. Bot. (Lond.)* **125**, 345 (2020).

[29] Z. Hu, T. Suzuki, T. Zitman, W. Uittewaal, and M. Stive, Laboratory study on wave dissipation by vegetation in combined current–wave flow, *Coastal Eng.* **88**, 131 (2014).

[30] C. W. Li and K. Yan, Numerical investigation of wave–current–vegetation interaction, *J. Hydraul. Eng.* **133**, 794 (2007).

[31] Z. Yin, Y. Wang, Y. Liu, and W. Zou, Wave attenuation by rigid emergent vegetation under combined wave and current flows, *Ocean Eng.* **213**, 107632 (2020).

[32] J. L. Lara, M. Maza, B. Ondiviela, J. Trinogga, I. J. Losada, T. J. Bouma, and N. Gordejuela, Large-scale 3-d experiments of wave and current interaction with real vegetation. Part 1: Guidelines for physical modeling, *Coastal Eng.* **107**, 70 (2016).

[33] I. J. Losada, M. Maza, and J. L. Lara, A new formulation for vegetation-induced damping under combined waves and currents, *Coastal Eng.* **107**, 1 (2016).

[34] M. Maza, J. L. Lara, I. J. Losada, B. Ondiviela, J. Trinogga, and T. J. Bouma, Large-scale 3-d experiments of wave and current interaction with real vegetation. Part 2: Experimental analysis, *Coastal Eng.* **106**, 73 (2015).

[35] M. Paul, T. Bouma, and C. Amos, Wave attenuation by submerged vegetation: Combining the effect of organism traits and tidal current, *Mar. Ecol. Prog. Ser.* **444**, 31 (2012).

[36] J. L. Garzon, M. Maza, C. M. Ferreira, J. L. Lara, and I. J. Losada, Wave attenuation by spartina saltmarshes in the Chesapeake Bay under storm surge conditions, *J. Geophys. Res. Oceans* **124**, 5220 (2019).

[37] C. Zhao, J. Tang, and Y. Shen, Experimental study on solitary wave attenuation by emerged vegetation in currents, *Ocean Eng.* **220**, 108414 (2021).

[38] X. Zhang, P. Lin, and H. Nepf, A simple wave damping model for flexible Marsh plants, *Limnol. Oceanogr.* (to be published).

[39] Z. Chen, C. Jiang, and H. Nepf, Flow adjustment at the leading edge of a submerged aquatic canopy, *Water Resour. Res.* **49**, 5537 (2013).

[40] J. Lei and H. Nepf, Evolution of flow velocity from the leading edge of 2-d and 3-d submerged canopies, *J. Fluid Mech.* **916**, A36 (2021).

[41] R. J. Lowe, J. R. Koseff, and S. G. Monismith, Oscillatory flow through submerged canopies: 1. Velocity structure, *J. Geophys. Res.: Oceans* **110**, C10016 (2005).

[42] R. B. Zeller, F. J. Zarama, J. S. Weitzman, and J. R. Koseff, A simple and practical model for combined wave-current canopy flows, *J. Fluid Mech.* **767**, 842 (2015).

[43] M. Luhar and H. M. Nepf, From the blade scale to the reach scale: A characterization of aquatic vegetative drag, *Adv. Water Res.* **51**, 305 (2013).

[44] See Supplemental Material at <http://link.aps.org/supplemental/10.1103/PhysRevFluids.6.100502> for the experimental measurements, the in-canopy time-mean and wave orbital velocity predicting method, and the force model validation, which includes Refs. [19,39–43,48].

[45] G. H. Keulegan and L. H. Carpenter, Forces on cylinders and plates in an oscillating fluid, *J. Res. Natl. Bur. Stand.* **60**, 423 (1958).

[46] X. Zhang and P. Lin, Wave-induced force on flexible marsh plants, *Chin. J. Theor. Appl. Mech.* **53**, 1018 (2021).

[47] H. Chen, Y. Ni, Y. Li, F. Liu, S. Ou, M. Su, Y. Peng, Z. Hu, W. Uijttewaal, and T. Suzuki, Deriving vegetation drag coefficients in combined wave-current flows by calibration and direct measurement methods, *Adv. Water Res.* **122**, 217 (2018).

[48] X. Zhang and H. Nepf, Reconfiguration of and drag on Marsh plants in combined currents and waves, *J. Fluids Struct.* (unpublished).

[49] F. J. Mendez and I. J. Losada, An empirical model to estimate the propagation of random breaking and nonbreaking waves over vegetation fields, *Coastal Eng.* **51**, 103 (2004).

[50] R. A. Dalrymple, J. T. Kirby, and P. A. Hwang, Wave diffraction due to areas of energy dissipation, *J. Waterway, Port, Coastal, Ocean Eng.* **110**, 67 (1984).

[51] D. G. Goring and V. I. Nikora, Despiking acoustic Doppler velocimeter data, *J. Hydraul. Eng.* **128**, 117 (2002).

[52] V. Nikora and D. Goring, Flow turbulence over fixed and weakly mobile gravel beds, *J. Hydraul. Eng.* **126**, 679 (2000).

[53] S. G. Monismith, E. A. Cowen, H. M. Nepf, J. Magnaudet, and L. Thais, Laboratory observations of mean flows under surface gravity waves, *J. Fluid Mech.* **573**, 131 (2007).

[54] L. A. Leonard and M. E. Luther, Flow hydrodynamics in tidal marsh canopies, *Limnol. Oceanogr.* **40**, 1474 (1995).

[55] A. F. Lightbody and H. M. Nepf, Prediction of velocity profiles and longitudinal dispersion in salt marsh vegetation, *Limnol. Oceanogr.* **51**, 218 (2006).

[56] Y. Xu and H. Nepf, Measured and predicted turbulent kinetic energy in flow through emergent vegetation with real plant morphology, *Water Resour. Res.* **56**, e2020WR027892 (2020).

[57] R. O. Tinoco Lopez, An experimental investigation of drag and the turbulent flow structure in simulated and real aquatic vegetation, Ph.D. thesis, Cornell University, Ithaca, NY, 2011.